

MAGELLAN ADAPTIVE OPTICS IMAGING OF PDS 70: MEASURING THE MASS ACCRETION RATE OF A YOUNG GIANT PLANET WITHIN A GAPPED DISK

KEVIN WAGNER^{1,2,3,*}, KATHERINE B. FOLLETTE⁴, LAIRD M. CLOSE¹, DÁNIEL APAI^{1,3,5,6}, AIDAN GIBBS¹, MIRIAM KEPPLER⁶, ANDRÉ MÜLLER⁶, THOMAS HENNING⁶, MARKUS KASPER⁷, YA-LIN WU⁸, JOSEPH LONG¹, JARED MALES¹, KATIE MORZINSKI¹, AND MELISSA MCCLURE⁹

Draft version August 31, 2024

ABSTRACT

PDS 70b is a recently discovered and directly imaged exoplanet within the wide ($\gtrsim 40$ au) cavity around PDS 70 (Keppler et al. 2018, Müller et al. 2018). Ongoing accretion onto the central star suggests that accretion onto PDS 70b may also be ongoing. We present the first high contrast images at H α (656 nm) and nearby continuum (643 nm) of PDS 70 utilizing the MagAO system. The combination of these filters allows for the accretion rate of the young planet to be inferred, as hot infalling hydrogen gas will emit strongly at H α over the optical continuum. We detected a source in H α at the position of PDS 70b on two sequential nights in May 2018, for which we establish a false positive probability of $< 0.1\%$. We conclude that PDS 70b is a young, actively accreting planet. We utilize the H α line luminosity to derive a mass accretion rate of $\dot{M} = 10^{-8 \pm 1} M_{Jup}/yr$, where the large uncertainty is primarily due to the unknown amount of optical extinction from the circumstellar and circumplanetary disks. PDS 70b represents the second case of an accreting planet interior to a disk gap, and is among the early examples of a planet observed during its formation.

Subject headings: Stars: pre-main sequence (PDS 70) — planets and satellites: formation — planets and satellites: detection — planet-disk interactions

1. INTRODUCTION

While gapped (“transition” and “pre-transition”) disks around young stars are fundamental to inform planet formation and disk evolution models (e.g., D’Angelo et al. 2003, Kley & Nelson 2012, Uribe et al. 2013), so far the link to planet formation has lacked significant direct evidence. With rapidly advancing instrumentation (e.g., Macintosh et al. 2006, Close et al. 2008, Beuzit et al. 2008) it is now possible to place (often powerful) constraints on massive planets interior to gapped disks around nearby young stars.

At young ages ($\lesssim 100$ Myr), giant planets are hot and luminous enough for their continuum thermal emission to be detectable in the infrared (e.g., Mordasini et al. 2017). Indeed, on the order of a dozen super-Jupiters have been discovered in recent years orbiting nearby young stars (see the recent review by Bowler 2016). Meanwhile, at very young ages ($\lesssim 10$ Myr), giant planets may still be accreting gas from the local disk environment. During active accretion epochs, the shocked hot ($\sim 10,000$ K) infalling Hydrogen gas may generate a significant and observable H α luminosity (Zhu 2015; Eisner 2015) that can easily boost planet-to-star contrast ratios to higher levels than in the infrared. Furthermore, a detection at H α also enables a mass accretion rate to be derived from empirical accretion rate vs. line luminosity rela-

tions (e.g., Rigliaco et al. 2012), thereby enabling planet formation to be observed as a time dependent process. This is the motivation behind the high-contrast H α capabilities of the Magellan Adaptive Optics System (Close et al. 2012, Morzinski et al. 2016) on the 6.5-m Magellan Clay Telescope, its flagship Giant Accreting Protoplanet Survey (GAPlanetS: Follette et al., *submitted*), and the H α capabilities of the Very Large Telescope’s Spectro-Polarimetric High Contrast Exoplanet Research Experiment (VLT/SPHERE). The power of this approach has already been demonstrated with MagAO’s detection of H α from the accreting protoplanet LkCa 15b (Sallum et al. 2015).

PDS 70 is a K7 pre-main sequence T Tauri type star in the Upper Centaurus Lupus association (Riaud et al. 2006, Pecaut & Mamajek 2016). The star hosts a gapped disk of moderate inclination ($i \sim 50^\circ$), with the gap extending from $\lesssim 17$ au to 60 au. This region ($\sim 0''.2$ to $0''.6$) is directly accessible to the high-contrast search zones of current adaptive optics (AO) systems (Hashimoto et al. 2012, Dong et al. 2012, Long et al. 2018), providing motivation for direct imaging searches to test the hypothesis that PDS 70’s gap has been cleared by the recent formation of one or more giant planets, as generally predicted by Dodson-Robinson & Salyk (2011).

Indeed, an on-going survey using VLT/SPHERE has recently discovered thermal emission from a giant planet interior to the disk’s gap (Keppler et al. 2018, Müller et al. 2018). The planet is confirmed in multiple photometric bands, with multiple telescopes and instruments, and in multiple epochs. In this configuration, PDS 70b is likely responsible for clearing and maintaining the gap, thereby driving its own mass accretion. A detection of PDS 70b in H α would enable a mass accretion rate to be estimated for the young planet, which has only been

¹ Steward Observatory, University of Arizona

² National Science Foundation Graduate Research Fellow

³ NASA NExSS *Earths in Other Solar Systems* Team

⁴ Department of Physics and Astronomy, Amherst College

⁵ Lunar and Planetary Laboratory, University of Arizona

⁶ Max Planck Institute for Astronomy, Heidelberg, Germany

⁷ European Southern Observatory, Garching, Germany

⁸ Department of Astronomy, University of Texas, Austin

⁹ University of Amsterdam, Netherlands

* Correspondence to: kwagner@as.arizona.edu

performed for one other exoplanet (LkCa 15b: Sallum et al. 2015, Follette et al. *submitted*).

2. OBSERVATIONS AND DATA REDUCTION

We observed PDS 70 using MagAO’s visible (VisAO: Males et al. 2014, Close et al. 2014) camera on 2017 Feb 10 as part of the GAPlanetS program (PI: Follette) and on two nights of general observing time (PI: Wagner) on 2018 May 3, and 2018 May 4. Each of our three observations was executed in the angular and spectral differential imaging plus mode (SDI+, Close et al. 2018). The new mode utilizes a spinning half wave plate in the fore-optics to randomize and effectively equalize any polarized disk signals in either beam, which then cancel along with the diffraction pattern in the spectral differential imaging (SDI) step.

In general, each observing sequence consisted of 1–2 hours of dithered observations. The conditions were excellent ($\sim 0''.5$ seeing) and the amount of field rotation was $\sim 90^\circ$ on each night. The core of PDS 70 was unsaturated in each of our exposures, enabling efficient field centering and frame-by-frame photometric calibration. Despite similar conditions, in 2017 the *R-I*-band brightness of PDS 70 measured by the wavefront sensor was 44% fainter in both $H\alpha$ and continuum filters. The All Sky Automated Survey for SuperNovae (Jayasinghe et al. 2018) has established a variability amplitude that is similar to or exceeding 40% for PDS 70 within the past year, so it is reasonable to assume that the different brightness observed by MagAO in 2017 vs. 2018 may be intrinsic. This decrease in brightness and corresponding decrease in AO performance likely precluded the detection of such a faint companion at $H\alpha$ in Feb 2017.

The raw data were dark-subtracted, divided by the instrumental flat field, and divided by the detector integration time of 30 seconds (45 sec for Feb 2017). The frames were aligned via cross-correlation with bi-linear interpolation to account for sub-pixel shifts. The position of PDS 70 was found via a Gaussian fit to the median PSF, and a second centering step was then performed utilizing the rotational symmetry of the PSF. This second step resulted in less than half of a pixel correction ($\lesssim 4$ mas) compared to the Gaussian fit. The accuracy of this method is estimated to be typically around $\lesssim 0.25$ pixels, or $\lesssim 2$ mas (Morzinski et al. 2015). We performed a frame selection based on the counts at the PSF core of PDS 70, and iterated upon this parameter with the presence of injected planets to arrive at the optimal value to maximize the SNR at $0''.2$. This resulted in rejecting frames whose core was less than (100,150,100) counts/s on 2017 Feb 10, 2018 May 3, and 2018 May 4, respectively, which correspond to (23%, 48%, 43%) of frames being rejected, and total integration times of (109,68,82) minutes.

The cubes were PSF subtracted through two independent algorithms: 1) classical angular differential imaging (cADI: Marois et al. 2006) and 2) projection onto eigenimages (Karhunen-Loève Image Processing, or KLIP: Soummer et al. 2012) via self-developed IDL scripts (Apai et al. 2016). Prior to cADI, the individual images were high-pass filtered by subtracting a 11×11 pixel (square) median-smoothed version of the image. For KLIP, we modelled and subtracted the PSF in six annular segments in the radial range of $0''.1$ – $0''.3$ from PDS 70, and iterated upon the remaining parameters in the

presence of injected planets (similar to the strategy outlined in Meshkat et al. 2014). The parameters that we explored for KLIP included high-pass filter width, minimum and maximum reference angle separation, and number of principal components. We arrived at optimal values of high-pass filter width = (15, 13, 17) pixels, minimum reference angle = $(1.1, 3.3, 5.5)^\circ$, maximum reference angle = $(40, 40, 45)^\circ$, and number of principal components = (5, 4, 4), for the three sequential epochs.

Following either PSF subtraction, the cubes were derotated and combined with a noise-weighted mean, which assigns lower weights to individual pixels with higher noise in the final derotated and combined image (Bottom et al. 2017). The $H\alpha$ and continuum images were then convolved with the measured width of the PSF (FWHM ~ 7 pixels). The continuum image was magnified by a factor of 656/643 (2% to account for radial scaling of the diffraction pattern with wavelength) and then the flux was scaled by the ratio of the peak counts of the median $H\alpha$ PSF to the median continuum PSF. The final SDI+ images were generated by subtracting the scaled continuum image from the $H\alpha$ image.

We also processed the data through a third pipeline, the GAPlanetS pipeline, which is described in detail in Follette et al., *submitted*. This pipeline provides a complete independent reduction from start to finish (notably, the cADI and KLIP pipelines mentioned above share the same initial processing). Briefly, the GAPlanetS pipeline includes dark current subtraction, flat fielding, cosmic ray rejection, rotational symmetry based star-centering, and utilizes the public pyKLIP package for PSF subtraction (Wang et al. 2015). The PSF subtraction is similar to our previously described KLIP pipeline with the exception that there is no maximum rotation angle imposed upon the reference library. Optimization of PyKLIP parameters was done by maximizing the signal to noise ratio of planets injected into the continuum images. We utilized the first two principal components in the PSF subtraction as this maximized the SNR of the injected planets, and note that the result is not significantly affected by the choice of between 1-50 principal components.

3. RESULTS

We detected a tentative (~ 2 – 3σ) $H\alpha$ point source in the May 3 data following an initial reduction of the data on the morning following the observations. We obtained the position angle and separation of the planet candidate identified by Keppler et al. through private communication and determined that the source identified in $H\alpha$ was in the location of PDS 70b. We observed the source again the following night, and obtained a consistent detection, which combined with the data from the night before yielded a more significant detection ($\sim 4\sigma$, see Fig. 1). The comparison of the output from our three data reduction pipelines is shown in Fig. 2. The individual channels are shown in Fig. 3 and Fig. 4 for May 3 and 4, respectively.

While no source is obvious in the single 2017 epoch, it would have been very near to the detection limit (likely due to the faintness of the star in 2017 and weaker AO performance), and we estimate a $\sim 50\%$ probability that a source of equal brightness would not have been detected. Thus, we consider only the higher quality 2018 data in

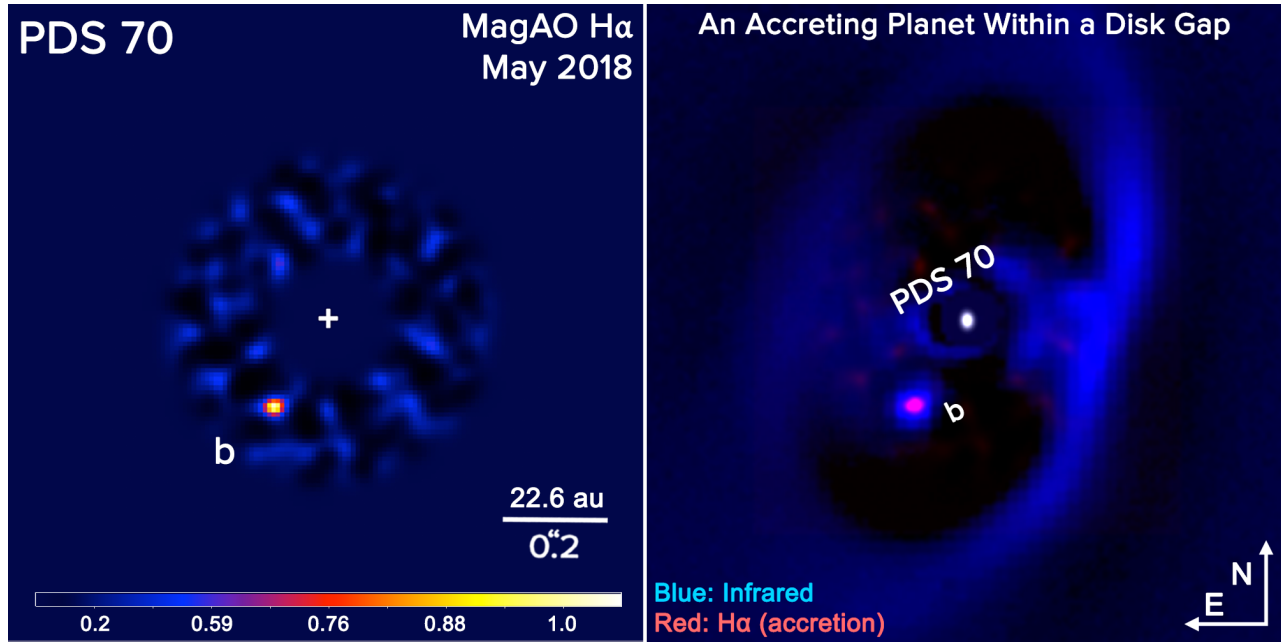


FIG. 1.— Left: MagAO $H\alpha$ SDI+ image of PDS 70. PDS 70b is the only clearly detected point source at $>95\%$ confidence. Right: Schematic false color diagram of the components of the PDS 70 system. The image is assembled from the $H\alpha$ image tracing accretion onto the planet (red) and the infrared image (blue) showing the planet’s thermal emission and starlight scattered by the disk (Müller et al. 2018). Note that the primary star also has $H\alpha$ emission that is not shown here due to the difficulty in capturing the extreme contrast ratio.

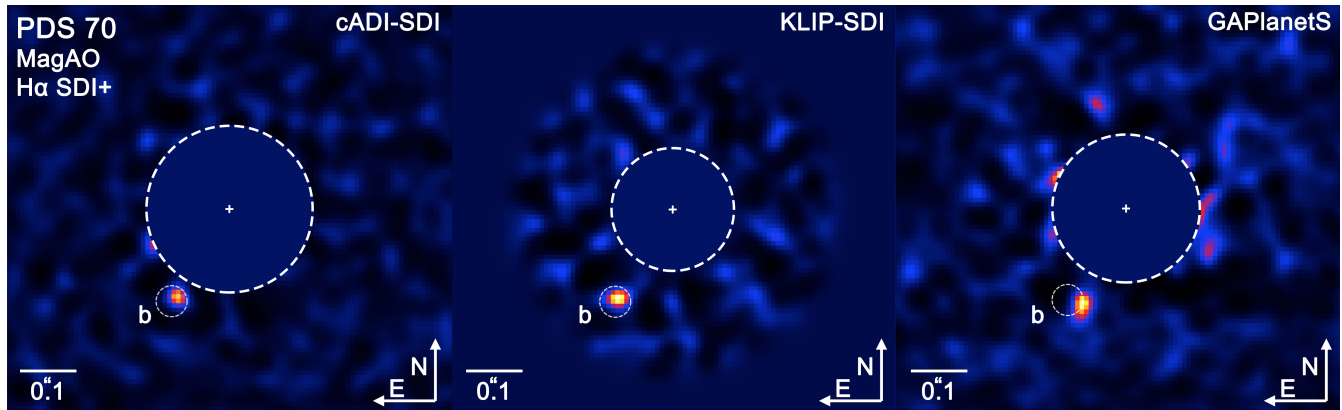


FIG. 2.— 2018 May 3/4 MagAO $H\alpha$ SDI+ data reductions utilizing cADI for the angular step (left), utilizing KLIP-ADI (center), and utilizing the GAPlanetS pre-processing and pyKLIP+SDI pipeline (right). All three methods yield a consistent detection of PDS 70b. The smaller dashed white circle (diameter = FWHM) indicates the most recent position of PDS 70b in Müller et al. (2018), which is consistent with the $H\alpha$ detection’s position in each pipeline (see the discussion on astrometric uncertainties in §3.1). The color scale is normalized and identical to that in the left panel of Fig. 1.

the proceeding analysis. While all three pipelines provide consistent results, the following analysis is based on our KLIP+SDI pipeline (Apai et al. 2016, center panel Fig. 2) in which PDS 70b is detected at the highest SNR.

3.1. Astrometry of PDS 70b

We measured astrometry via centroiding on the source, and established uncertainties through repeating the analysis on injected planets to establish measurement uncertainties. We converted image coordinates to on-sky positions via a platescale calibration of 7.851 ± 0.015 mas/pixel and true North calibration of $0.9^\circ \pm 0.3^\circ$ E of N (Close et al. 2013). On May 3 we detected PDS 70b at a separation of 183 ± 18 mas and position angle (PA) of $148.8^\circ \pm 1.7^\circ$. On May 4, we detected PDS 70b at a separation of 193 ± 12 mas and PA of $143.4^\circ \pm 4.2^\circ$.

Both of these positions are consistent within $1-\sigma$ of each other and with the most recent SPHERE astrometry of 192 ± 8 mas separation and PA of $147^\circ \pm 2.5^\circ$ (Müller et al. 2018).

3.2. $H\alpha$ Luminosity of PDS 70b and the Mass Accretion Rate of a Growing Planet

On each night and in the combined data we compared the flux in a 5-pixel radius aperture centered on PDS 70b to the mean and standard deviation of identical measurements carried out on the injected planets to measure the $H\alpha$ contrast (and uncertainty) of PDS 70b. On May 3 and 4 we measured contrasts of PDS 70b in $H\alpha$ to the optical continuum of $1.04 \pm 0.70 \times 10^{-3}$, and $1.40 \pm 0.66 \times 10^{-3}$, respectively. In the combined image, we measured a contrast of $1.14 \pm 0.47 \times 10^{-3}$. The

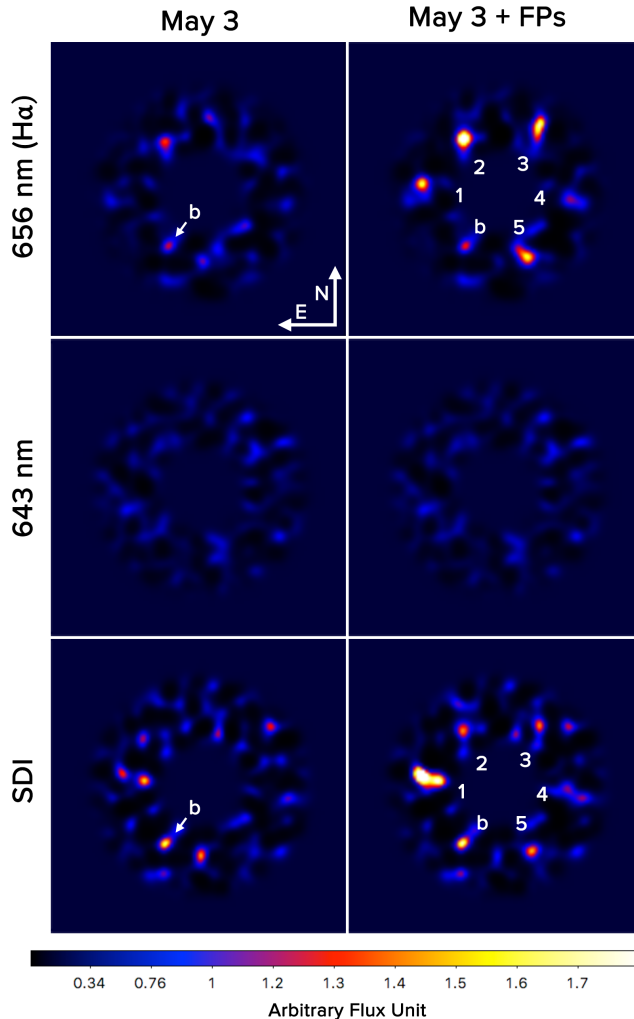


FIG. 3.— 2018 May 3 continuum, H α , and H α – continuum (SDI) images (left column), and the same data with five injected planets (FPs) at 1.5×10^{-3} contrast (right column).

contrasts listed above correspond to the brightness ratio of PDS 70b in H α to PDS 70 in the adjacent continuum. This non-standard definition of contrast is chosen for the reason that it eliminates the need to correct for variable accretion onto PDS 70 as well as the star’s variable chromospheric activity. While the star is also optically variable, between the two nights we measured less than 5% variability in both filters, which is substantially smaller than the photometric measurement uncertainties for PDS 70b, and hence no correction for optical variability of PDS 70 is needed.

Following the strategy in Close et al. (2014), we converted the H α luminosity to a mass accretion rate. Briefly, the calculation follows the conversion from H α luminosity, to accretion luminosity, to accretion rate as outlined in Rigliaco et al. (2012). The R -band apparent brightness of the star is somewhat uncertain (~ 0.4 mag) and we adopt here $R=11.7$ (Henden et al. 2015). We also assume a planetary radius equivalent to that of Jupiter, a mass of $5\text{--}9 M_{Jup}$ planet (Keppler et al. 2018), and taking into account our photometric uncertainty, calculate a mass accretion rate of $\dot{M}_{PDS70b} = 10^{-8.7 \pm 0.3} M_{Jup}/yr$.

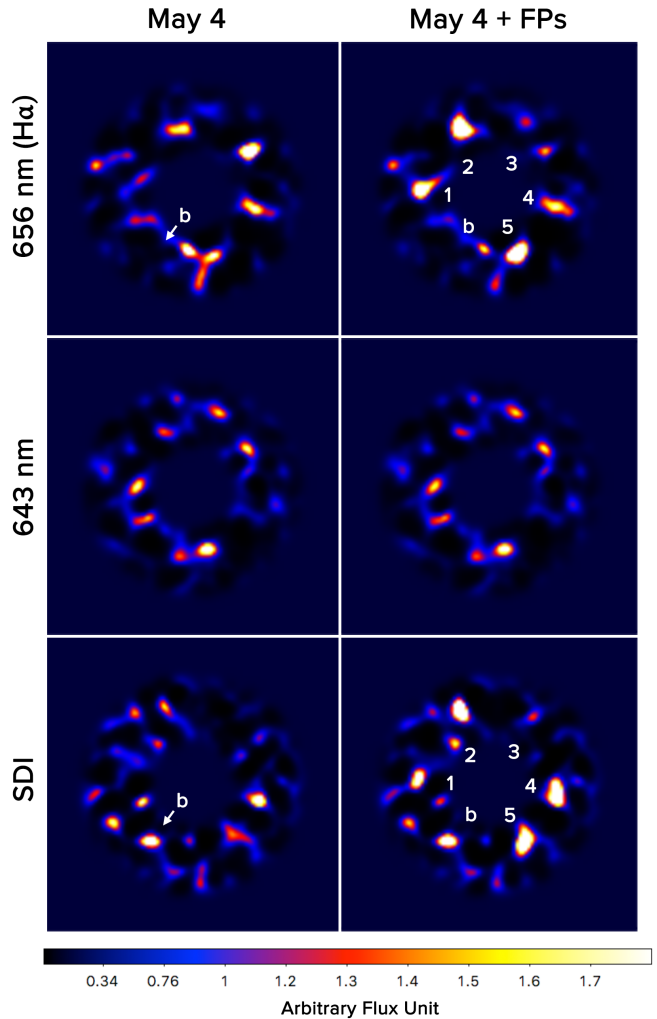


FIG. 4.— 2018 May 4 continuum, H α , and H α – continuum (SDI) images (left column), and the same data with five injected planets (FPs) at 1.5×10^{-3} contrast (right column).

To account for a different radius of PDS 70b, the mass accretion rates listed here should simply be multiplied by $R_{PDS70b}/R_{Jupiter}$. For illustrative purposes, we account for up to 3.0 mags of optical extinction from the circumplanetary+circumstellar disks and interstellar medium, as well as the wider mass range found in Müller et al. (2018), and find a plausible range for the mass accretion rate of $\dot{M}_{PDS70b} = 10^{-8 \pm 1} M_{Jup}/yr$ (see Fig. 5). Note that in this example the lower limit is still dominated by the measurement uncertainties, but the substantial amount of extinction significantly raises the upper limit to $10^{-7} M_{Jup}/yr$. While this choice of extinction is arbitrary, it is not extreme, especially if the circumplanetary disk is viewed at a significant inclination.

4. DISCUSSION

4.1. Probability of a False Positive Result

To establish the probability of a false positive detection on both nights in 2018, we analyzed the spatial distribution of speckles in the final SDI+ images. Over the image area between $0''.1\text{--}0''.3$ from PDS 70, we counted the speckles of similar brightness to the point source at

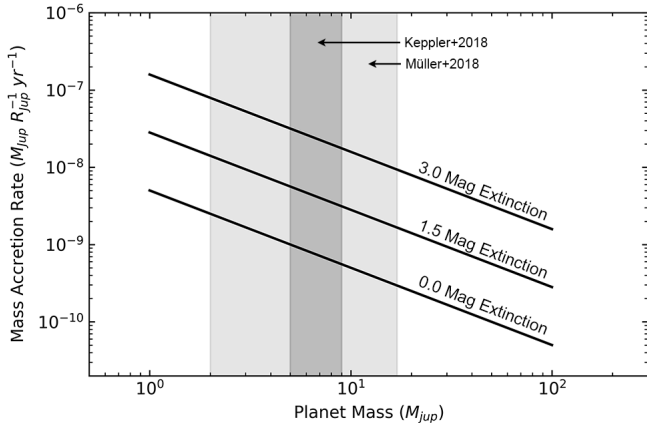


FIG. 5.— The scaling relation of PDS 70b’s mass accretion rate with planet mass and extinction. The mass ranges of Kepler et al. (2018) and Müller et al. (2018) are displayed in the shaded regions.

the position of PDS 70b (including the source itself), and found seven such sources for May 3, and twelve for May 4, which are approximately equivalent to 25 and 50 speckles per square arcsecond. These are conservative estimates, as PDS 70b is actually the brightest source in each image and we considered anything of similar brightness to include all sources within a factor of two of its flux to be a plausible false positive.

To be wrongly considered a detection of PDS 70b, a speckle must not only share a consistent brightness, but must also fall within $\sim 2\sigma$ of the planet’s location. We estimated the area corresponding to a 2σ astrometric uncertainty through the recovered astrometry of our injected planets, and found this area to be ~ 0.00043 square arcseconds for May 3 and 0.00072 square arcseconds for May 4. Combined with the speckle densities, these translate into (conservative) false positive probabilities for either night of 1.1% and 3.6% for May 3 and 4, respectively, and a combined probability of $\sim 4 \times 10^{-4}$ for a speckle of the same brightness to appear within 2σ of the known location of the object on both nights. Given that the individual detections of PDS 70b fall within 1σ of the recent SPHERE astrometry, rather than the 2σ criteria considered above, a less conservative estimate may be more appropriate. In this case, the area in question for a speckle to randomly land is reduced by a factor of four, and so is the corresponding false-positive probability.

Confidence in the astrophysical nature of the $H\alpha$ emission from PDS 70b also comes from the significance of the detection in the combined May 3/4 dataset, in which PDS 70b is the only clearly detected source. We estimated the signal to noise ratio by comparing the flux in a $1 \times \text{FWHM}$ wide aperture compared to the noise measured in all other non-overlapping apertures at the same radius from the star. We followed Equation 9 in Mawet et al. (2014) to estimate the SNR, taking into account the correction for small sample statistics at ~ 3.5 beam widths from the star. This resulted in 20 independent noise measurements, compared to which the detection of PDS 70b stands out as a 3.9σ outlier in the combined 2018 data. Via the same analysis, PDS 70b stands out at 2.6σ and 2.4σ on May 3 and 4, respectively. As expected for a real source, the SNR improves roughly as

the square root of the total exposure time. The corresponding false positive probability is thus $\sim 10^{-4}$ in the combined image, or around 1% on either night—in excellent agreement with the analysis above.

4.2. A Giant Planet Caught in Formation

The $H\alpha$ emission from PDS 70b indicates that the object is still accumulating mass from its surrounding disk environment. Thus, it is still in the process of formation, and its current mass and mass accretion rate can be used to estimate the final mass that PDS 70b will attain. Considering that PDS 70b has already gained on the order of $\sim 10 M_{Jup}$ in mass, it is unlikely that PDS 70b will grow even an additional $\sim 10\%$ of its mass within the disk dispersal lifetime, even at the upper limit of its mass accretion rate of $10^{-7} M_{Jup} \text{yr}^{-1}$. Unless the extinction is extremely high, it is unlikely that the accretion rate is higher than the value considered here. In other words, in absence of a dramatic increase in the accretion rate, or extreme cases of optical extinction, it appears that PDS 70b has reached its isolation mass.

We may also make some inferences about the formation history of the young planet by performing the calculation in reverse. Even at its upper limit of $10^{-7} M_{Jup} \text{yr}^{-1}$, PDS 70b would have taken at least 20 Myr to grow to its minimum mass estimate of $2 M_{Jup}$ (Müller et al. 2018). This is four times longer than the system’s estimated age (Müller et al. 2018). Thus, to attain its minimum mass in the estimated 5 Myr age of the system, we infer that the accretion rate would have needed to be at least (on average) a modest four times higher than the maximum value considered here.

These inferences are consistent with a formation scenario for PDS 70b in which the planet experienced a period of run-away gas accretion. During this epoch the planet likely (at least partially) played a role in clearing the wide gap that it currently resides in. It is interesting, then, that the planet continues to accrete gas and emit strongly at $H\alpha$. Similar to LkCa 15b (Sallum et al. 2015), the fraction of material accreting onto PDS 70b is comparable to the amount of accretion onto the star ($\dot{M}_{PDS70} \lesssim 10^{-8} M_{Jup} \text{yr}^{-1}$; Long et al. 2018 and private communication). This suggests that the planet may play a role in shepherding material through the disk gap and onto the star, meanwhile accreting some fraction of this material onto itself. Indeed, Kepler et al. (2018) and Müller et al. (2018) identify several structures extending interior to the gap that may be related to planet-driven spiral waves or other disk transport processes.

5. SUMMARY AND CONCLUSIONS

We have observed PDS 70b on three nights throughout Feb 2017 to May 2018 with MagAO in the $H\alpha$ SDI+ mode on the 6.5-*m* Magellan Clay telescope at Las Campanas Observatory, Chile. On sequential nights in 2018, we detected a point source in $H\alpha$ at $\sim 10^{-3}$ contrast to the star. Both independent detections in 2018 are at a level of $\sim 2-3\sigma$, and combined yield a $\sim 4\sigma$ detection. In 2017, the observations were not sensitive enough to confidently detect the planet.

Both detections in 2018 are consistent within 1σ of the other’s astrometry, and with the most recent SPHERE astrometric measurement of PDS 70b. We explored the probability that the detection of PDS 70b on both nights

is a random false positive through two independent methods, and arrive at a consistent false alarm probability of $\sim 10^{-4}$. We conclude that the detected H α emission originated from PDS 70b.

We converted the object's H α contrast in 2018 to a mass accretion rate, assuming the range of masses for PDS 70b in Keppler et al. (2018) and Müller et al. (2018), and several cases of extinction, and found a mass accretion rate of $\dot{M} = 10^{-8\pm 1} M_{Jup}/yr$. Given the mass and mass accretion rate of PDS 70b, we estimate that the planet has already acquired $\gtrsim 90\%$ of its mass.

6. ACKNOWLEDGMENTS

The authors express their gratitude toward Korash Asani, Zachary Long, Michael Sitko, and Kaitlin Kratter for useful discussions that improved the quality of this work. The results reported herein benefited from col-

laborations and/or information exchange within NASA's Nexus for Exoplanet System Science (NExSS) research coordination network sponsored by NASA's Science Mission Directorate, and includes data gathered with the 6.5 meter Magellan Telescopes located at Las Campanas Observatory, Chile. We acknowledge the contributions of Clare Leonard, Alex Watson, Elijah Spiro, Wyatt Mullen and Raymond Nzaba to the GAPlanetS pipeline. KMM's and LMC's work is supported by the NASA Exoplanets Research Program (XRP) by cooperative agreement NNX16AD44G. A.M. acknowledges the support of the DFG priority program SPP 1992 "Exploring the Diversity of Extrasolar Planets" (MU 4172/1-1). L.M.C.'s research with MagAO was supported by the NSF ATI (Grant No. 1506818), the NSF AAG program #1615408, and the NASA XRP program 80NSSC18K0441.

REFERENCES

- Apai, D., Kasper, M., Skemer, A., et al. 2016, *ApJ*, 820, 40
 Beuzit, J.-L., Feldt, M., Dohlen, K., et al. 2008, *Proc. SPIE*, 7014, 701418
 Bottom, M., Ruane, G., & Mawet, D. 2017, *Research Notes of the American Astronomical Society*, 1, 30
 Bowler, B. P. 2016, *PASP*, 128, 102001
 Close, L. M., Gasho, V., Kopon, D., et al. 2008, *Proc. SPIE*, 7015, 70150Y
 Close, L. M., Males, J. R., Kopon, D. A., et al. 2012a, *Proc. SPIE*, 8447, 84470X
 Close, L. M., Males, J. R., Morzinski, K., et al. 2013, *ApJ*, 774, 94
 Close, L. M., Follette, K. B., Males, J. R., et al. 2014, *ApJ*, 781, L30
 Close, L. M., et al. 2018, *Proc. SPIE*, 10703, <https://arxiv.org/abs/1807.05070>
 D'Angelo, G., Kley, W., & Henning, T. 2003, *ApJ*, 586, 540
 Dodson-Robinson, S. E., & Salyk, C. 2011, *ApJ*, 738, 131
 Dong, R., Hashimoto, J., Rafikov, R., et al. 2012, *ApJ*, 760, 111
 Eisner, J. A. 2015, *ApJ*, 803, L4
 Hashimoto, J., Dong, R., Kudo, T., et al. 2012, *ApJ*, 758, L19
 Henden, A. A., Levine, S., Terrell, D., & Welch, D. L. 2015, *American Astronomical Society Meeting Abstracts #225*, 225, 336.16
 Jayasinghe, T., Kochanek, C. S., Stanek, K. Z., et al. 2018, *MNRAS*, 477, 3145
 Keppler, M., Benisty, M., Müller, A., et al. 2018, [arXiv:1806.11568](https://arxiv.org/abs/1806.11568)
 Kley, W., & Nelson, R. P. 2012, *ARA&A*, 50, 211
 Long, Z. C., Akiyama, E., Sitko, M., et al. 2018, *ApJ*, 858, 112
 Macintosh, B., Graham, J., Palmer, D., et al. 2006, *Proc. SPIE*, 6272, 62720L
 Males, J. R., Close, L. M., Morzinski, K. M., et al. 2014, *ApJ*, 786, 32
 Marois, C., Lafrenière, D., Doyon, R., Macintosh, B., & Nadeau, D. 2006, *ApJ*, 641, 556
 Mawet, D., Milli, J., Wahhaj, Z., et al. 2014, *ApJ*, 792, 97
 Meshkat, T., Kenworthy, M. A., Quanz, S. P., & Amara, A. 2014, *ApJ*, 780, 17
 Mordasini, C., Marleau, G.-D., & Mollière, P. 2017, *A&A*, 608, A72
 Morzinski, K. M., Males, J. R., Skemer, A. J., et al. 2015, *ApJ*, 815, 108
 Morzinski, K. M., Close, L. M., Males, J. R., et al. 2016, *Proc. SPIE*, 9909, 990901
 Müller, A., Keppler, M., Henning, T., et al. 2018, [arXiv:1806.11567](https://arxiv.org/abs/1806.11567)
 Pecaut, M. J., & Mamajek, E. E. 2016, *MNRAS*, 461, 794
 Riaud, P., Mawet, D., Absil, O., et al. 2006, *A&A*, 458, 317
 Rigliaco, E., Natta, A., Testi, L., et al. 2012, *A&A*, 548, A56
 Sallum, S., Follette, K. B., Eisner, J. A., et al. 2015, *Nature*, 527, 342
 Soummer, R., Pueyo, L., & Larkin, J. 2012, *ApJ*, 755, L28
 Uribe, A. L., Klahr, H., & Henning, T. 2013, *ApJ*, 769, 97
 Wang, J. J., Ruffio, J.-B., De Rosa, R. J., et al. 2015, *Astrophysics Source Code Library*, [ascl:1506.001](https://arxiv.org/abs/1506.001)
 Zhu, Z. 2015, *ApJ*, 799, 16